https://doi.org/10.5194/bg-2021-68
Preprint. Discussion started: 22 March 2021

Biogeosciences Discussions
Open Access

How are oxygen budgets influenced by dissolved iron and growth of oxygenic phototrophs in an iron-rich spring system? Initial results from the Espan Spring in Fürth, Germany

Inga Köhler[1], Raul E. Martinez[2], David Piatka.[1], Achim J. Herrmann[3], Arianna Gallo[3], Michelle M. Gehringer[3], Johannes A.C. Barth[1]

[1]Department of Geography and Geosiences, GeoZentrum Nordbayern, Friedrich-Alexander-Universität FAU, Erlangen, 91054, Germany

[2]Max-Planck-Institute for Biogeochemistry, Jena, 07745, Germany

[3]Division of Microbiology, Technische Universität, Kaiserslautern, 67663 Germany

Correspondence to: Inga Köhler (inga_koehlergmx.de)

Abstract. At present most knowledge on the impact of iron on $^{18}O/^{16}O$ ratios (i.e. $\delta^{18}O$) of dissolved oxygen (DO) under circum-neutral conditions stems from experiments carried out under controlled laboratory conditions. These showed that iron oxidation leads to an increase in $\delta^{18}O_{DO}$ values**.** Here we present the first study on effects of elevated Fe(II) concentrations on the $\delta^{18}O_{DO}$ in a natural, iron-rich circum-neutral watercourse. Our results show that iron oxidation was the major factor dominating the oxygen isotopes in the first 85 meters of the system in the cold season (December/ February) and for the first 15 meters during the warm season (May). This trend existed despite a constant oxygen supply from the atmosphere. Further along the course of a spring and associated small stream system, the $\delta^{18}O_{DO}$ decreased towards values known for atmospheric equilibration. This may be due to reduced iron oxidation, increased atmospheric exchange and photosynthetic DO production. The presence of oxygenic phototrophic mats suggested their involvement in the observed decrease in $\delta^{18}O_{DO}$ values. In the cold season, the $\delta^{18}O_{DO}$ values stabilized around atmospheric equilibrium at +24.6 ‰, whereas in the warm season values decreased to +21.8 ‰. This suggests stronger influences by oxygenic photosynthesis. About 145 meters downstream of the spring, the $\delta^{18}O_{DO}$ increased again in the warm season until it reached the atmospheric equilibrium value of +24.6 ‰. This trend can be explained by a respiratory consumption of DO combined with a decrease in photosynthetic activity. Our study shows that dissolved Fe(II) can exert strong effects on the $\delta^{18}O_{DO}$ of a natural circum-neutral spring system even though a constant supply of atmospheric oxygen occurs. In the presence of active photosynthesis, with active supply of oxygen to the system, direct effects of Fe oxidation on the $\delta^{18}O_{DO}$ value becomes masked. However, critical Fe(II) concentrations may indirectly control DO budgets by enhancing photosynthesis, particularly if cyanobacteria are involved.

1 Introduction

Oxygen is the most abundant (45.2 %) and iron the fourth most abundant (5.8 %) element on earth (Skinner, 1979). Such huge global reservoirs render these elements critically important in global biogeochemical cycles. In addition, their reactivity is exceptional: O_2 is a powerful oxidation agent while Fe can cover oxidation states from –4 to +7 in extreme cases, with the most commonly known ones being 0, +2 and +3 (Lu et al., 2016).

Iron is also an essential trace element in many biological processes, including photosynthesis, oxygen transport and DNA biosynthesis (Kappler et al., 2021). This closely links to the formation and dissolution of Fe oxides that may enhance or reduce availabilities of both elements in the water column and pore waters and thus may largely regulate aqueous life.

In aqueous environments, dissolved oxygen (DO) is one of the most essential ecosystem parameters and, despite its moderate solubility (e.g. 9.3 mg L^{-1} at 20 °C), it assumes a central role in respiration, primary production and Fe-oxidation (Pusch, 1996). The concentration of DO coupled to its stable isotope $^{18}O/^{16}O$ ratios (i.e. $\delta^{18}O$) can

https://doi.org/10.5194/bg-2021-68
Preprint. Discussion started: 22 March 2021

yield additional information about sources and sinks, including atmospheric input, photosynthesis, respiration and mineral oxidation.

When equilibrated with the atmosphere, $\delta^{18}O_{DO}$ values typically range around a value of + 24.6 ‰ (Mader et al., 2017) while photosynthesis and respiration can change these isotope ratios (Guy et al., 1993; Kroopnick, 1975). The splitting of water molecules during photosynthesis hardly produces an isotope discrimination and the resulting DO has the same isotope value as the surrounding water (Guy et. al., 1993; Eisenstadt et al., 2010). Meteoric water in temperate climates is normally depleted in ^{18}O and therefore the photosynthetic oxygen in these areas varies between - 10 to – 5 ‰ (Quay et. al., 1995; Wang and Veizer, 2000). Respiration, on the other hand, accumulates ^{16}O and enriches the remaining DO in ^{18}O and yields $\delta^{18}O_{DO}$ values between + 24.6 and + 40 ‰ (Guy et. al., 1993). Additionally, oxidation of metals such as Fe also lead to a rise in $\delta^{18}O_{DO}$ (Lloyd, 1968; Taylor and Wheeler, 1984; Wassenaar and Hendry, 2007; Oba and Poulsen, 2009 a,b; Pati, 2016). Mostly, the impacts of Fe oxidation on $\delta^{18}O_{DO}$ values have been investigated experimentally under controlled conditions (Oba and Poulson, 2009b; Pati et al., 2016). However, so far these dynamics were not studied in open water systems such as springs and rivers. Variations in the fractionation factors obtained in the abovementioned studies resulted from differences in temperature, pH and initial Fe(II) concentrations that could be outlined under abiotic conditions.

Dissolved Fe(II) in natural systems may have primary and secondary impacts on DO concentration and its $\delta^{18}O_{DO}$ values. The primary influence originates from the O_2 binding by iron oxidation (equation 1). This leads to decreases of the DO and simultaneous increases of the $\delta^{18}O_{DO}$ value (Wassenaar and Hendry, 2007; Smith et al., 2011; Parker et al., 2012 and Gammons et al., 2014).

(1) $4\ Fe^{2+} + O_2 + 4\ H^+ \rightarrow 4\ Fe^{3+} + 2\ H_2O$

Dissolved Fe(II) can also have secondary (i.e. indirect) influences on the DO content and the $\delta^{18}O_{DO}$. This happens when it acts as an essential micronutrient to cause growth-stimulating effects on O_2-producing and respiring microorganisms.

Influence of Fe(II) on DO and $\delta^{18}O_{DO}$ in circum-neutral aquatic systems have so far received little attention because of the following reasons:

(1) Fe oxidation often masks $\delta^{18}O_{DO}$ values created by respiration, photosynthetic and atmospheric oxygen and

(2) adequate Fe(II)-rich circum-neutral model systems are scarce on modern earth. This is due to the high reactivity of iron with DO.

To the best of our knowledge, no study so far has systematically investigated the influences of elevated Fe(II) concentrations on $\delta^{18}O_{DO}$ values in a natural and circum-neutral iron-rich system. In order to bridge this gap, we investigated the aqueous chemistry and $\delta^{18}O_{DO}$ values in the iron-rich Espan spring in Fürth, Germany (Fig. 1). This Fe(II)-rich artesian spring offers a complex biogeochemical natural field site to analyse effects of different Fe(II) contents on the DO and $\delta^{18}O_{DO}$ values.

https://doi.org/10.5194/bg-2021-68
Preprint. Discussion started: 22 March 2021

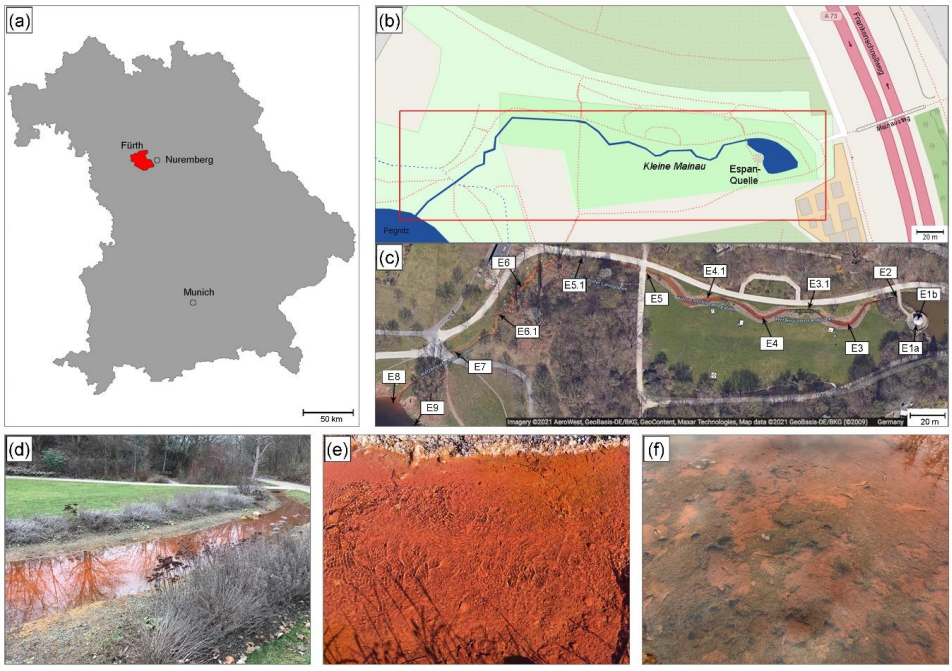

Figure 1 Overview over the Espan Spring in Fürth, Germany. a) and b): Location of the spring in Bavaria and the city of Fürth. c) Satellite image (© Google maps) of the spring showing the distinct red colour. d) to f) Detailed photos of the system. Image d) displays spring area between sampling points E4 and E5, image is shows sampling point E3 and image F displays sampling point E4.1.

The aims of this study were to establish an inventory of biology together with Fe and oxygen budgets in this exceptional natural spring and stream system. We further aimed to investigate how increased Fe(II)-levels influence the oxygen budget of the system and whether a combination of DO and $\delta^{18}O_{DO}$ measurements can help to asses this effect. This is also timely because environmental impacts of Fe(II) are increasingly being recognised as problematic. This is for instance the case with phenomena of browning or brownification (Kritzberg and Ekström, 2011; Weyhenmeyer et al., 2014; Kritzberg et al., 2020). During this process, increased iron levels can consume oxygen, cause algae blooms and reduce water potability and thus affect aqueous ecosystems and their services. Here we describe a first complete spatial sampling campaign with Fe(II), Fe(III), DO and its stable $^{18}O/^{16}O$ isotope ratios as well as field parameters from a cold season and warm season campaign. This study contributes to the knowledge of Fe oxidation in natural systems and implications of seasonal dynamics in Fe(II) rich systems.

2 Methods

2.1 Study site

The Espan Spring is located in the city of Fürth, Germany (49°28'15.8"N 11°00'53.0"E, Fig. 1). It is an artesian spring that originates from a confined aquifer that was tapped by a drilling project in 1935 from a depth of 448.5 m below ground. The water originates from the so called “lower mineral water horizon”, which is dominated by

https://doi.org/10.5194/bg-2021-68
Preprint. Discussion started: 22 March 2021

artesian inflow from the lower Buntsandstein Formation. After the water exits the well in a pavilion with a temperature of ~ 20 °C, it discharges into a stream of about 300 m length that is known as the "Wetzendorfer Landgraben (WL)" that drains into the Pegnitz River without any further tributaries (Fig. 1b, c). The water can be classified as a Na-Ca-Cl-SO_4 mineral water with initially undersaturated DO values of 2.3 mg/L and Fe(II) contents of up to 6.6 mg/L (Table 1). Figure 1C shows an aerial image of the spring and stream system that shows a distinct red coloring of the stream bed. The most plausible explanation is that this coloring originates from iron-precipitates (Fig. 1 d, e).

2.2 Sampling procedures

Two field campaigns were performed in February and May 2020, during which water was collected at 14 locations along the stream between 8 am and 12 pm. The water was collected at about 10 cm depth below the surface. The onsite parameters pH (±0.05; instrument precision), temperature (±0.1 °C), electrical conductivity, Eh and DO (all ±2 %) were measured with a HACH HQ 40d multi parameter instrument. Alkalinity titrations were carried out with a Hach Titrator with a bromocresol-green indicator. Fe(II) and Fe(III) contents were measured using an iron (II/III) cuvette test set by Hach in combination with a portable Hach spectrophotometer (model DR 2800).
Samples for $^{18}O/^{16}O$ ratios of DO were collected in 12-mL Exetainers® (Labco Ltd. Lampeter, U.K.) that were prepared with 10 µL of a saturated $HgCl_2$ solution to prevent secondary biological activity after sampling (Wassenaar and Koehler, 1999; Parker et al., 2005 and 2010). The Exetainers were filled with syringe-filtered water via 0.45 µm pore size nylon filters until they were entirely full and free of air bubbles. They were then carefully closed with screw caps with a butyl septum in order to avoid atmospheric contamination. Test series showed that the amount of atmospheric contamination during this filling procedure is usually negligible (Mader et al. 2018).
Samples for water isotopes were collected in 15 mL-Falcon tubes bottles and treated in the same manner as the ones for DO isotope measurements, except for preservation with $HgCl_2$. Instead, the samples were stored in a mobile refrigerator box at 4 °C directly after collection and carried to the laboratory where they were measured within 24 h.

2.3 Identification of possible mineral precipitates

In order to determine possible mineral precipitate data for the pH, pe, temperature, alkalinity (as $CaCO_3$), as well as cations and anions, the specific sampling points were fed into the program PhreeqC (Version 3; Parkhurst and Appelo, 2013) for calculation of saturation indices. The database used was Wateq4.

2.5 Laboratory methods

2.5.1 Identification of cyanobacteria

Samples were collected in a preliminary field assessment at the anoxic piping where the spring flows into the creek (E2), in the middle of the creek at first small pond after the water had contact to the atmosphere (E3) and about 5 m downstream of this pond from algal mat with bubbles on the surface (E4). Samples for cyanobacterial isolation were collected in sterile 2-mL- Sarsted tubes and sealed. Samples for microscopy were collected with a 75 % ethanol sterilised spatula and placed in a sterile 6 cm petri dish (Sarsted, Germany). Immediately after returning

https://doi.org/10.5194/bg-2021-68
Preprint. Discussion started: 22 March 2021

from the sampling site, samples were embedded in 1.5 % Agarose in de-ionized water to preserve the structure of the bio mats during further handling and shipping.
Microscopic analysis was performed on thin sections of the embedded mats using a CLSM-type microscope (LSM 880, Carl Zeiss), using modified acquisition settings from Jung *et al.* (2019) to discriminate between cyanobacterial (chlorophyll-*a* (chl-*a*) and phycobiliproteins (PBP)) and green algal (chl *a*) fluorescence. Laser transmission images were also generated using the 543 nm laser.

A spatula tip of green coloured mat was used to inoculate 5 mL of BG11 medium (Stanier et al., 1971) in a well of a 6-well plate incubated for 3 weeks at 24 °C on a 16:8 day:night cycle with illumination at 15 µmols photons m^2 s^{-1} under a OSRAM L30W/840 LUMINLUX Cool White bulbs. Individual Cyanobacterial species were picked from the mat cultures under a Nikon SMZ-U Zoom binocular microscope for further subculturing on 1% agar solidified BG11 plates, as well as liquid culture. Isolates were observed under an Olympus BX53 light microscope and their morphologies recorded using an Olympus DP26 Camera. The number of cells per filament and cell dimensions were measured using ImageJ 1.47v software. DNA was extracted (Gehringer et. al, 2010) from one axenic isolate of a microscopically identified *Persinema* species of cyanobacteria and the 16s rDNA gene and intergenic spacer sequence amplified by the SSU-4 fwd and ptLSU-C-D rev primer pair (Marin et al., 2005) using the Taq PCR mastermix (Qiagen, Germany). The cleaned PCR product (NucleoSpin PCR clean-up kit, Macherey-Nagel, Germany) and sequenced (Wilmotte et al., 1993). Sequences were merged (HVDR Fragment Merger tool, Bell & Kramvis, 2013) and the final 16S-ITS sequence submitted to NCBI.

2.5.2 Isotope measurements

Stable isotope ratios of DO (expressed as $\delta^{18}O_{DO}$) were measured on a Delta V Advantage Isotope Ratio Mass Spectrometer (IRMS; Thermo Fisher Scientific, Bremen, Germany) coupled to an automated equilibration unit (Gasbench II). Measurements were carried out in continuous flow mode with a modified method by Barth et al. (2004). Here the isolation of DO into a headspace relies on a helium extraction technique by Kampbell et al. (1989) and Wassenaar and Koehler (1999). Different portions of laboratory air were injected into helium-flushed Exetainers® and used to correct obtained data sets for linearity and instrumental drift during each run. Data were normalized to laboratory air.

$$\delta = (R_{sample} / R_{SMOW} - 1) \qquad \text{(Clark and Fritz, 1997)}$$

To obtain ratio changes in per mille (‰), the δ values were multiplied by factor of 1000.
All samples were measured in triplicates and isotope values standard deviations (1σ) were less than 0.1 and 0.2 ‰ for $\delta^{18}O_{H2O}$ and $\delta^{18}O_{DO}$, respectively.

3 Results and discussion

3.1 On-site parameters

The on-site parameters as displayed in Table 1 show a range of pH values between 6.1 and 8.6 in the cold season

https://doi.org/10.5194/bg-2021-68
Preprint. Discussion started: 22 March 2021

Sampling point	Distance from spring (m)	pH	O_2 (mg/L)	Temperature (°C)	Conductivity (mS/cm)	Alkalinity (mg/L)	Fe^{2+} (mg/L)	Fe^{3+} (mg/L)	Na^{+} (g/L)	Ca^{2+} (g/L)	SO_4^{2-} (g/L)	Cl^{-} (g/L)	U^{6+} (µg / L)
Cold season													
E1a	0	6.1	2.3	19.5	16.8	820	6.6	0.4	2.5	1.2	2.1	4.4	170
E1b	0	6.5	3.4	19.3	16.4	828	6.6	0.4	2.5	1.2	2.2	4.5	170
E2	15	6.5	4.5	19.3	16.5	796	5.6	0.4	2.5	1.2	2.2	4.5	170
E3	45	6.7	5.8	17.5	16.8	790	5.7	0.4	2.5	1.2	2.2	4.5	170
E3.1	65	6.5	7.4	17.3	16.6	810	4.5	0.5	2.5	1.2	2.2	4.5	170
E4	85	7.1	8.0	16.2	16.9	804	3.9	0.6	2.5	1.2	2.2	4.5	170
E4.1	115	7.5	8.7	16.1	17.0	808	3.4	0.6	2.5	1.2	2.2	4.5	170
E5	145	7.9	8.9	15.2	16.8	804	0.9	0.8	2.4	1.2	2.2	4.5	170
E5.1	175	7.6	9.1	15.3	16.8	816	0.4	0.5	2.5	1.2	2.2	4.5	170
E6	205	7.9	9.5	14.1	16.9	760	0.2	0.1	2.5	1.2	2.2	4.5	170
E6.1	235	7.9	9.7	13.3	16.5	770	0.0	0.1	2.5	1.2	2.2	4.5	170
E7	265	8.0	10.1	12.3	16.6	760	0.0	0.1	2.4	1.1	2.2	4.5	170
E8	295	8.0	10.5	10.8	1.1	195	0.0	0.1	0.1	0.1	0.1	0.2	5.0
E9	300	8.6	11.0	7.4	0.5	160	0.0	0.1	0.0	0.1	0.0	0.0	0.4
Warm season													
E1a	0	6.3	3.6	21.3	16.3	874	6.9	0.0	2.4	1.1	2.2	4.5	190
E1b	0	6.4	3.9	21.2	16.4	850	6.7	0.1	2.5	1.1	2.2	4.4	190
E2	15	6.5	5.9	20.6	16.4	846	5.6	0.0	2.5	1.1	2.1	4.4	160
E3	45	6.6	6.6	21.6	16.4	814	4.0	0.0	2.4	1.1	2.2	4.4	160
E3.1	65	6.9	7.6	22.5	16.4	808	2.9	0.1	2.4	1.1	2.2	4.4	160
E4	85	7.2	8.2	22.7	16.4	826	1.5	0.1	2.5	1.1	2.2	4.4	160
E4.1	115	7.3	8.0	23.0	16.4	812	0.7	0.2	2.5	1.1	2.2	4.5	160
E5	145	7.4	8.1	24.0	16.4	786	0.1	0.1	2.4	1.1	2.2	4.5	160
E5.1	175	7.5	8.0	25.6	16.4	804	0.0	0.0	2.5	1.1	2.2	4.5	160
E6	205	7.5	8.1	25.7	16.4	796	0.0	0.0	2.5	1.1	2.2	4.5	160
E6.1	235	7.5	7.9	25.5	16.4	748	0.0	0.0	2.4	1.1	2.2	4.5	150
E7	265	7.5	8.1	24.9	16.4	742	0.0	0.0	2.5	1.1	2.2	4.5	150
E8	295	7.5	8.3	22.8	16.4	708	0.0	0.0	2.5	1.1	2.2	0.3	180
E9	300	8.0	8.8	16.8	0.8	238	0.0	0.0	0.1	0.1	0.0	0.0	1.0

https://doi.org/10.5194/bg-2021-68
Preprint. Discussion started: 22 March 2021

Table 1 On-site parameters, major ion concentrations and Fe(II) as well as DO concentrations for the Espan Spring. Note that values before the forward slash are for cold season and after the slash for warm season

and between 6.3 and 8.0 in the warm season. The changes of the pH over the course of the spring are due to the constant degassing of CO_2 from the spring. Oxygen values rise from 2.3 mg/L to 11.0 mg/L in the cold season and from 3.6 mg/L to 8.8 mg/L in the warm season. Differences between the cold and warm season are due to the fact that *cold* water can hold more dissolved *oxygen than warm water***.** The general rise in the amount of dissolved oxygen over the course of the spring is due to a continuous dissolution of atmospheric oxygen in the spring water and due to the impact of photosynthesis. The water temperatures range between 19.3- 7.4°C in the cold season and between 21. 3 to 25.7°C in the warm season. The changes in temperature can be explained by an equilibration with the air temperatures thus dropping in the cold and rising in the warm season. The conductivity remained relatively stable over the course of the spring and only showed minor differences between the cold and warm season. The same applies to the alkalinity. The behaviour of the Fe(II) and Fe(III) are described in section 3.5. Values of cations and anions remain constant over the course of the spring and show no differences between the cold and warm season.

3.2 Precipitation calculations

Precipitating mineral phases as determined with PhreeqC showed that the dominant phase at all measurement points is Hematite (Fe_2O_3) (Supplementary Information Table 1). Additionally, Goethite (α-FeO(OH)), Ferrihydrite ($Fe(OH)_3$), Siderite ($FeCO_3$) and K-Jarosite ($KFe^{3+}{}_3(OH)_6(SO_4)_2$) as well as $CaCO_3$ and Rhodochrosite ($MnCO_3$) showed elevated SI values to enable precipitation.

3.3 Bacterial contents

CLSM showed that only the samples from Site E4.1 have photosynthetic organisms in significant quantities during the cold period. The photosynthetic community in this biofilm was dominated by cyanobacteria, with very few eukaryotic algae (Fig. 2).

https://doi.org/10.5194/bg-2021-68
Preprint. Discussion started: 22 March 2021

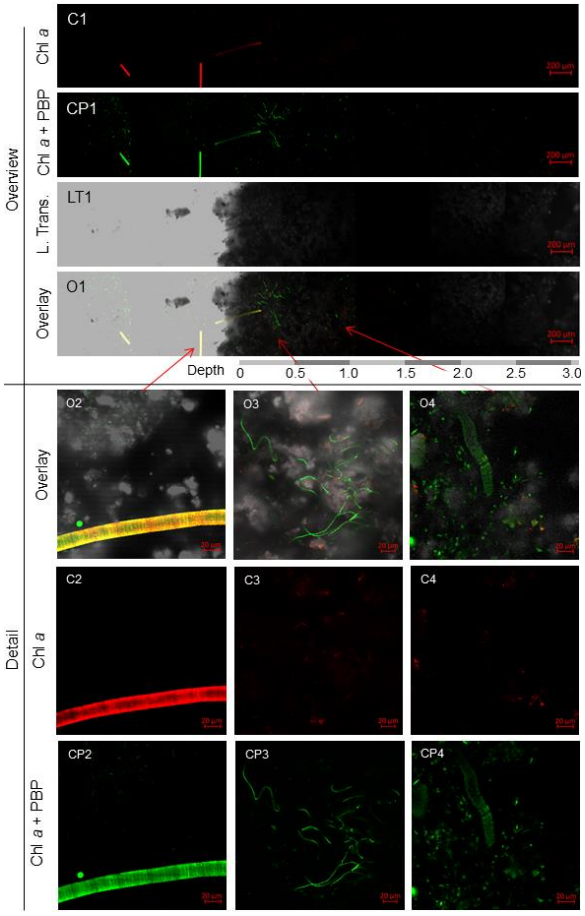

Figure 2 CLSM images of mat sample E4.1. Overview**:** images of the cross-section of the top 3 mm of the biofilm with the Chl-a (C1) and chl-a plus PBP (CP1) fluorescence profile, complemented by a laser transmission picture (LT1) and the superimposed image (O1). **Detail:** Superimposed images (O2/3/4) of Chl a (C2/3/3) and Chl a plus PBP (CP2/3/4) fluorescence and laser transmission (not shown) of distinct organisms found in the bio mat. **O2**: eukaryotic algae. **O3**: Possible Klisinema- or Persinema–like sp. and a unicellular cyanobacterium. **O4**: Lynbya –like sp. and a unicellular cyanobacterium.

Most of the cyanobacteria and all eukaryotic algae were located in the topmost 1.2 mm of the biofilms (Fig. 2 O1). Close-up images show eukaryotic algae (Fig. 2.O2), thin filamentous cyanobacteria, possibly *Persinema sp.* or *Klisinema sp.*(Fig. 2.O3) and *Lynbya* sp. (Fig. 2.O4). All pictures of the top layers of this sample site show an abundance of unidentified unicellular cyanobacteria, while images from the other sample sites show very few photosynthetic organisms at all (supplementary material 1).

To determine the identity of the predominant cyanobacterial species isolated from the E4.1 enrichment cultures, a determination key (Komárek und Anagnostidis, 2005) was used to compare particular features of an isolate to those already in the literature for specific cyanobacterial species. Note that enrichment cultures for samples E2 and E3 did not yield enough material for cyanobacterial determination after 5 weeks in culture.

https://doi.org/10.5194/bg-2021-68
Preprint. Discussion started: 22 March 2021

The red-brown filamentous strain (Fig. 3, c & d) exhibits single filaments, without false branching, that are 30.9 to 38.2 µm wide (Table 2), with a firm, 9.5 to 14 µm thick sheath. The trichomes and single cells are 21.5 to 24.2 µm wide and 1.5 to 4.1 µm long (Table 2), are red-brown in colour and constricted at the cross-walls. Based on these characteristics, the species was attributed to the cyanobacterial genus *Lyngbya*.

	Filament length	Filament width (µm)	Cell width (µm)	Cell length (µm)
Lyngbya sp.	Indeterminate	30.9 – 38.2	21.5 – 24.2	1.5 – 4.1
Klisinema sp.	Indeterminate	3.9 – 7.6	12 – 4.5	0.3 – 0.4
Persinema. sp	Indeterminate		0.5 – 1.8	2.7 – 4.7

Table 2 Filament and cell dimensions of the proposed cyanobacterial species.

The blue-green filamentous strain (Fig. 3, b) produces single filaments, without false branching, that are 3.9 – 7.6 µm wide (Table 2) with a firm, 2.7 – 3.1 µm thick sheath. The trichomes and single cells are 1.2 – 4.5 µm wide and 0.3 – 0.4 µm long (Table 2), blue-green in colour, no constriction at the cross-walls. The terminal cells in mature filaments are conical, elongated and bent to one side, corresponding to those of the *Klisinema* genus recently described by Heidari et al. (2018). The thin, naked pale green filaments (Figure 3a & e) resembled those of *Persinema komarekii* (Heidari et al., 2018) with apical cells flattened at the end. In contrast to the observations of Heidari et al. (2018), we observed terminal aerotopes. This species was purified in culture and the 16S-ITS (NCBI accession number: MT708471) sequence confirmed its identity to *Persinema komarekii* (MF348313).

https://doi.org/10.5194/bg-2021-68
Preprint. Discussion started: 22 March 2021

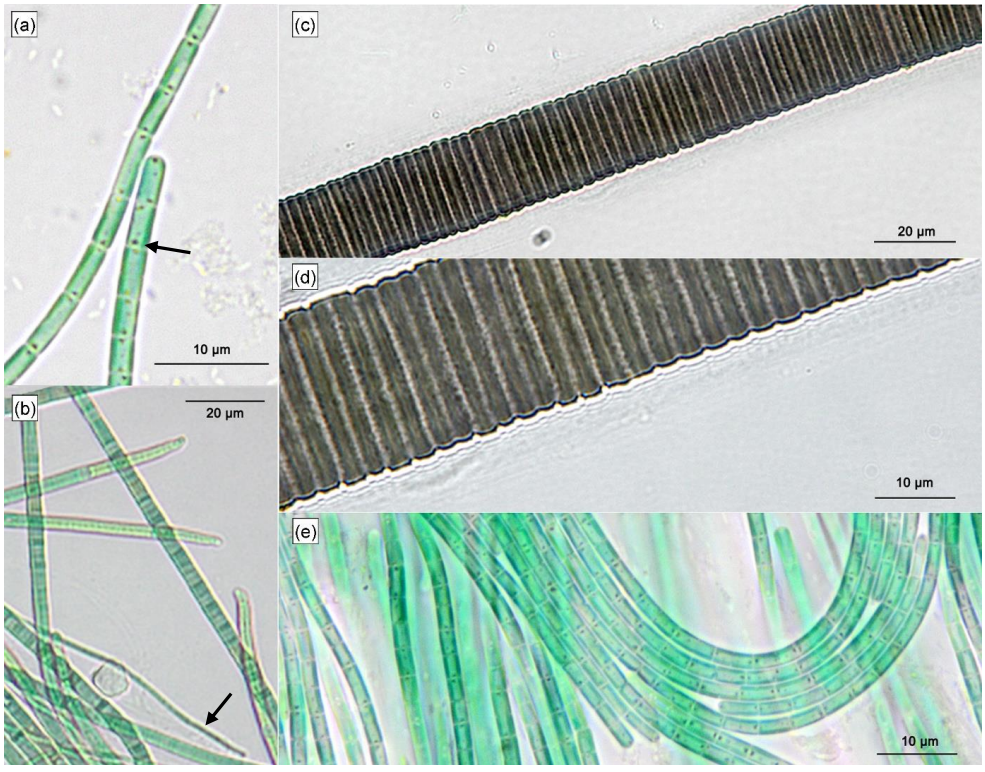

Figure 3 Light Micrographs of the predominant isolates from sample E4.1: a) Single filament of *Persinema sp.*, arrow indicates aerotopes. B) Biofilm of *Klisinema sp.* interspersed with *Persinema sp* (arrow) c) *Lyngbya sp.*, filament d) *Lyngbya sp* sheath detail, E: Biofilm of *Persinema sp.*

3.4 Dissolved oxygen

The DO concentration in the Espan System was lowest at the faucet in the Pavilion (sampling point E1a) with a saturation of 25.3 % (2.3 mg/L) (Fig. 4a). Over the next 100 meters DO saturation rose to 88.1 % (8.7 mg/L) in sampling point E4.1. Afterwards the saturation continually rose to 94.6 % (11.0 mg/L) in point E8. From an initial depth of 435 meters with the abundance of reduced species such as Fe(II) and Mn(II), the low DO content in sampling point E1a was expected. In the further course, more atmospheric oxygen was able to dissolve. Bubbles were observed in association with the *Lyngbya* mats. They were most prominent at sample site E4.1 and indicate a significant contribution of O_2 from daytime photosynthesis. However, saturation with DO was not reached during neither of the sampling campaigns.

https://doi.org/10.5194/bg-2021-68
Preprint. Discussion started: 22 March 2021

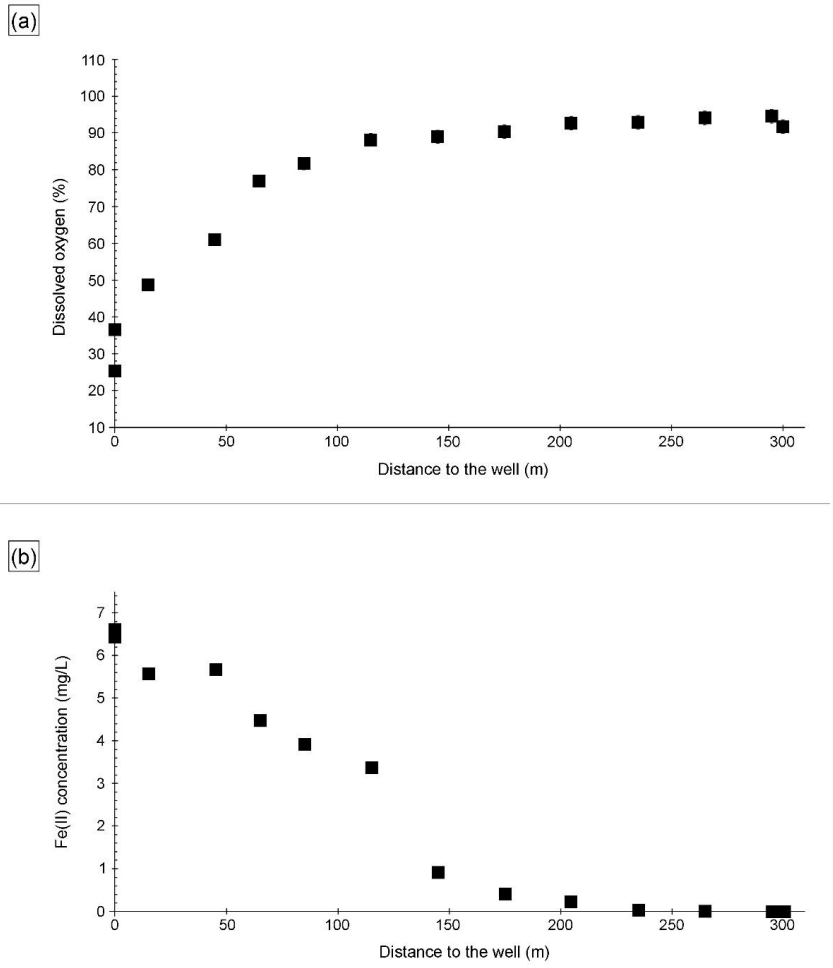

Figure 4 a) Dissolved oxygen (%) and b) Fe(II) concentrations over the course of the Espan system (cold season). The error for DO was 2 % and for Fe(II) it was 0.06 mg/L. Errors are within symbol size.

3.5 Fe(II) and Fe(III)

The Fe(II) content was highest at the faucet with 6.6 mg/L while its lowest content was below instrument precision. at sampling point E9 at 300 meters from the source (Fig. 4b). Fe(II) concentrations decreased constantly over the stream course and were accompanied by increases in DO saturation (Fig. 4a). The decrease in Fe(II) could have been caused by three major processes:

(1) Oxidation of Fe(II) to form ferric iron minerals such as ferrihydrite, hematite and goethite

(2) Precipitation of Fe(II) minerals such as the iron carbonate siderite ($FeCO_3$) and/or an amorphous ferrous silicate phase or

(3) Adsorption of Fe(II) on already formed iron minerals.

https://doi.org/10.5194/bg-2021-68
Preprint. Discussion started: 22 March 2021

All three possibilities seem plausible when taking into consideration the saturation indices of ferric iron minerals, goethite, ferrihydrite and hematite precipitate at all sampling points in the system (Köhler et al. 2020). These calculations furthermore show that siderite can precipitate in almost all sampling points while iron-silicate minerals are unlikely to precipitate. Therefore, adsorption of Fe (II) onto minerals should be possible in the Espan System. Such adsorption of Fe(II) onto (oxyhydr)oxides was shown to typically occur under neutral conditions and should increase with rising pH (Zhang et al.,1992; Liger et al., 1999; Appelo et al., 2002; Silvester et al., 2005). The observed high dissolved Fe(II) content of the spring system at circum-neutral pH, and rising DO concentrations, can be explained by the occurrence of large amounts of sulphate (~2.2 g/L) and chloride (~4.5 g/L). These elevated parameters can delay abiotic Fe(II) oxidation (Millero, 1985).

Dissolved Fe(III) was highest (0.8 mg/L) at sampling point E5 after 145 m and lowest (0.05 mg/L) at sampling point E7 after 265 m flow distance from the spring. The values initially rose from 0.4 mg/L in E1a to a maximum of 0.8 mg/L in point E5 (+/- 0.03 mg/L) and then decreased to the lowest value in E7. The solubility of iron oxides in natural systems at a circum-neutral pH and under aerobic conditions is generally very low (Cornell and Schwertmann, 2003) with values of the solubility product (K_{sp}) between 10^{-37} and 10^{-44} (Schwertmann, 1991). However, Fe(III) could still be detected in the water, thus showing that its dissolution was possible. The dissolution of iron oxides can occur through several pathways including as protonation, reduction and complexation that create Fe(III) cations, Fe(II) cations as well as Fe(II) and Fe(III) complexes (Schwertmann, 1991; Cornell and Schwertmann, 2003). Both the protonation as well as the reduction would lead to the formation of dissolved Fe(II). Steep increase in dissolved Fe(III) at 145 m downstream of the spring (from 0.5 mg/L to 0.8 mg/L) also indicates acceleration of this process. One reason for this increase could be available organic matter. However, further analyses are needed to verify this interpretation.

3.6 $\delta^{18}O_{DO}$

Figure 5 a) and b) show $\delta^{18}O_{DO}$ values over the course of the spring for the cold and warm seasons, respectively. The curves are divided into two zones for the cold season and three zones for the warm season. A zone was defined by the increase or decrease of the $\delta^{18}O_{DO}$ values.

Zone 1

In the cold season, zone 1 extended from sampling point E1a to point E4. In these first 85 meters, the $\delta^{18}O_{DO}$ rose from a value of +23.7 ‰ at the faucet (E1a) to + 25.7 ‰ at E4. In the warm season, zone 1 extended from E1a to E2 at only 15 m distance from the spring. In this zone the values rose from + 23.4 ‰ at the faucet to a maximum value of + 24.7 ‰ at E2. In both seasons, $\delta^{18}O_{DO}$ values at E1a were below the value expected for atmospheric equilibration (+ 24.6 ‰). At first sight such light $\delta^{18}O_{DO}$ values would suggest photosynthetic input of DO. However, the water did not have any contact with light and thus any photosynthetic influence can be ruled out.

The occurrence of $\delta^{18}O_{DO}$ values below + 24.6 ‰ in groundwater has been described in the literature (Wassenaar and Hendry, 2007; Smith et al., 2011; Parker et al., 2014 and Mader et al, 2018) and several explanations for this phenomenon have been suggested (Wassenaar and Hendry, 2007; Smith et al., 2011; Parker et al., 2014 and Mader et al, 2018). These include:

(1) possible transfer of photosynthetic or diffusive oxygen into the shallow aquifer (Smith et. al; 2011; Parker et al., 2014; Mader et al., 2018),

https://doi.org/10.5194/bg-2021-68
Preprint. Discussion started: 22 March 2021

(2) radial oxygen loss of plant roots (Teal and Kanwisher, 1966; Michaud and Richardson, 1989; Caetano and Vale, 2002; Armstrong and Armstrong, 2005b)

(3) radiolysis of water (Wassenaar and Hendry, 2007) and

(4) kinetic gas transfer (Benson and Krause, 1980; Knox et al. ,1992, Mader et al. 2017)

Explanations (1) and (2) are very unlikely in the Espan Spring, because the water originates from a depth of 435 meters below ground, through pipes that presumably prevent any exchange with surface water or possible impacts of plant roots. It should be noted that water from the Espan Spring contains up to 170 µg/L of uranium from easily soluble uranium compounds that are commonly encountered in the Buntsandstein formations. The geogenic radiation in the area is additionally rather high because of the high uranium content in the Variscian bedrocks of the area (Schwab, 1987; Büttner et al., 2006). Because of this, radiolysis could be a possible explanation for the unexpected low $\delta^{18}O_{DO}$ values. Kinetic gas transfer of atmospheric oxygen during transport in the pipes or at the faucet might be the most likely explanation, since the sample in E1a is strongly DO undersaturated. During non-equilibrium gas exchange the kinetically faster ^{16}O would cause $\delta^{18}O_{DO}$ values lighter than 24.6 ‰ until equilibrium establishes (Benson and Krause, 1980; Knox et al. ,1992, Mader et al. 2017).

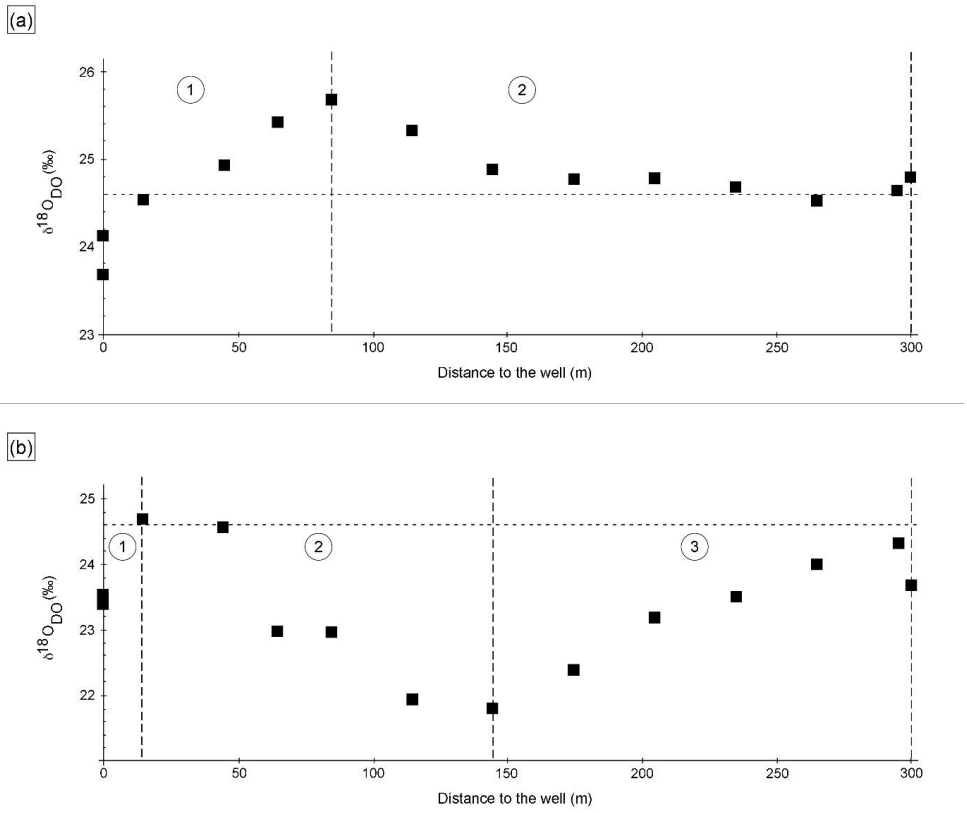

Figure 5 $\delta^{18}O_{DO}$ in the cold season a) and the warm season b) over the course of the Espan system with the atmospheric equilibrium value of + 24.6 ‰ marked by the horizontal line. Dashed vertical lines show borders of the different zones of the curves labelled with 1, 2 and 3. The symbol size is larger than the error bars.

https://doi.org/10.5194/bg-2021-68
Preprint. Discussion started: 22 March 2021

Increases in $\delta^{18}O_{DO}$ values in zone 1 were accompanied by increases in DO (Fig. 6a). In the cold season, a strong positive correlation was evident between points E1a and E4. However, in the warm season, the same correlation could be observed between points E1a and E2 (Fig. 6b). Through equilibration with the atmosphere, this trend would be reasonable until atmospheric equilibration was reached between point E2 and E3. However, the $\delta^{18}O_{DO}$ values, at least in the cold season, increased above this threshold to a value of + 25.7 ‰. In the warm season, the atmospheric equilibrium was only marginally exceeded and remained within the range of the analytical uncertainties. This shows that another process in addition to atmospheric equilibration must have influenced the $\delta^{18}O_{DO}$ values in zone 1.

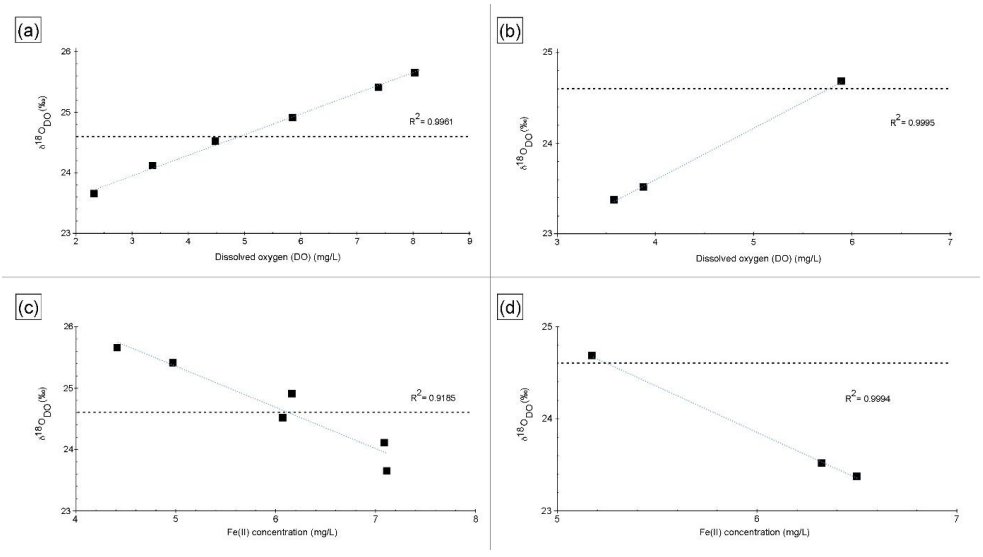

Figure 6 Correlation between $\delta^{18}O_{DO}$ and DO over the course of the spring for zone 1 in the cold season a) and the warm season b). Correlation between $\delta^{18}O_{DO}$ and Fe(II) contents over the course of the stream for zone 1 in the cold season c) and the warm season d).

Even though these processes consume DO, both respiration and iron oxidation could be responsible for this trend when assuming that they influence the $\delta^{18}O_{DO}$ values, while DO concentrations are constantly replenished by the atmosphere. Notably, a direct negative correlation between Fe(II) concentrations and $\delta^{18}O_{DO}$ values between point E1a and E4 was evident for cold season samples and in point E1a and E2 for warm season samples as shown in Figure 6c and d. This correlation between Fe(II) and $\delta^{18}O_{DO}$ in the Espan System corresponds with the experimental observations of Oba and Poulson (2009), as well as those of Pati et al. (2016). These studies demonstrate that Fe oxidation leads to increases in $\delta^{18}O_{DO}$ values due to preferential consumption of ^{16}O. The increase in $\delta^{18}O_{DO}$ due to iron oxidation in a natural system, which is constantly supplied with fresh oxygen, indicates that Fe(II) oxidation must be the dominant control on $\delta^{18}O_{DO}$ in the first 85 meters of the stream in the cold season and in the first 15 meters in warm season. It also implies that the direct impact of oxygen addition is subordinate in terms of DO stable isotope changes.

Zone 2

https://doi.org/10.5194/bg-2021-68
Preprint. Discussion started: 22 March 2021

In the cold season, zone 2 extended from sampling point E4 to point E9 and only minor variations in $\delta^{18}O_{DO}$ could be found. In this zone, the $\delta^{18}O_{DO}$ decreased from + 25.7 ‰ in sampling point E4 to values around atmospheric equilibrium with + 24.5 ‰ in E7 and + 24.8 ‰ in the Pegnitz River (Fig. 5a).

In the warm season, zone 2 extended from sampling point E2 to point E5 at 145 meters from the spring. In this zone the values decreased from + 24.7 ‰ to a minimum value of + 21.8 ‰ in point E5 (Fig. 5b). This decrease in $\delta^{18}O_{DO}$ values can be explained by (1) a decrease of the impact of iron oxidation on the $\delta^{18}O_{DO}$ values and (2) a rising impact of atmospheric or photosynthetic oxygen. Even though a decrease in Fe(II) values was still evident between E4 and E7 in the cold season, as well as between E2 and E5 in the warm season, it is possible that the decrease was not caused by Fe(II) oxidation and subsequent precipitation as iron oxides. Alternatively the decrease could have been caused by adsorption of dissolved Fe(II) onto already existing iron oxides such as goethite, ferrihydrite and hematite (Zhang, et al., 1992; Liger et al., 1999; Appelo et al., 2002; Silvester et al. 2005). Because adsorbed Fe(II) is very resistant to oxidation (Park and Dempsey, 2005) the impact of iron oxidation on the $\delta^{18}O_{DO}$ values would decrease.

The question remains why an increased adsorption would occur specifically downstream of points E2 and E4. No significant changes in the water chemistry were evident and it can be assumed that after sampling point E2 (warm season) or E4 (cold season), a critical value is exceeded with enough Fe(II) having been adsorbed onto iron oxides that iron oxidation --- while probably still taking place at small rates--- is no longer the factor dominating the $\delta^{18}O_{DO}$ values. Downstream of point E2 and E4 oxygen addition would thus be the dominating factor.

Because intensive growth of cyanobacterial and algal mats (Fig. 1f) were observed between point E3.1 and E5 in the cold season and between E3 and E5 in the warm season, it can be postulated that, in addition to the atmospheric O_2 input, the $\delta^{18}O_{DO}$ values were also influenced by addition of photosynthetically produced oxygen. While this effect should be less pronounced in the cold and darker season, a strong influence of photosynthetic oxygen on the $\delta^{18}O_{DO}$ values should be possible in the warm season with higher light intensity.

Considerable growth of photosynthetic organisms in the Espan System is not surprising with iron being an important micronutrient (Andrews et al., 2003).

The fact that photosynthesising organisms seem to preferentially grow and impact the $\delta^{18}O_{DO}$ values between sampling point E3 and E5 may be due to the availability of Fe(II). The growth could also be due to changes in the pH or other environmental influences, with the site being located in a public park with the associated perturbations. Cyanobacteria, especially aquatic strains prefer a neutral to alkaline pH (Brock, 1973) and the shift to higher pH values in this zone could be one of the main factors that drive increased supply of cyanobacterial O_2.

A screening of microbial ecology in several iron-rich circum-neutral springs and experiments with the cyanobacterium *Synechococcus* PCC 7002 (Swanner et al. 2015a) revealed that many cyanobacteria show optimal growth between 0.4 – 3.1 mg/L Fe(II) and that concentrations above 4.5 mg/L become growth-limiting. The iron concentrations between point E3.1 and E5 in cold season and E3 and E5 in warm season are thus approximately in the range of optimal cyanobacterial growth. In order to establish a clear correlation between the iron concentration and the decrease in $\delta^{18}O_{DO}$ values, experiments need to be carried out with the organisms found in the Espan System. These have so far have not been assessed for their behaviour under variable iron concentrations.

Zone 3

In the warm season, zone 3 extended from sampling point E5 to point E8. In this zone the $\delta^{18}O$ values rose again from + 21.8 ‰ to + 24.3 ‰ (Fig. 5B). The renewed increase in values can be explained by the influence of iron

https://doi.org/10.5194/bg-2021-68
Preprint. Discussion started: 22 March 2021

oxidation, respiration and a decrease in photosynthetic activity. Because Fe contents only decreased marginally, it can be assumed that decreases in photosynthetic activities are responsible for increase in the $\delta^{18}O$ values. This matches our observations that downstream of point E5, only little or no photosynthetic growth could be observed. Oxygen that would dissolve in the water after point E5 would thus most likely stem from the atmosphere. This would explain the approach to the equilibrium value of + 24.6 ‰. Reasons for the observed decrease in cyanobacteria are not clear however, they may include changes in temperature, light intensity and shifts in nutrient availability.

The temperature did not change significantly in this part of the watercourse and is therefore unlikely to have caused a decrease in photosynthetic oxygen production. In contrast, reduced light exposure can in fact be responsible as downstream of point E5 trees shade the spring. A decrease in nutrient availability is difficult to determine because nitrate and phosphate were below the detection limit in the entire spring. Iron starvation could also be a possible reason for the decrease in activity because only ~0.005 mg/L Fe(II) was left in the system in the later course of the stream. In order to outline these processes future studies should target laboratory experiments with the photosynthetic organisms found.

4 Conclusions

Our study is the first systematic analyses of $\delta^{18}O_{DO}$ values as a function of iron contents and oxygenic photosynthetic biofilms in a natural iron-rich spring. We were able to confirm from field samples that Fe-oxidation leads to increases in $\delta^{18}O_{DO}$ values even though oxygen was constantly replenished by atmospheric input. As soon as photosynthetic oxygen is produced in the system, the effect of iron oxidation on the $\delta^{18}O_{DO}$ values becomes negligible and cannot hardly be detected any longer. The fact that photosynthesis has a strong impact on the $\delta^{18}O_{DO}$ values in specific areas of the system may be controlled by high Fe contents of the system. Similar iron-rich springs show optimal growth rates of cyanobacteria in the range of 0.4 – 3.1 mg/L Fe(II). The presented $\delta^{18}O_{DO}$ values showed that photosynthetic activity is also strongest in the Espan System within this range of concentrations.

To what extent the cyanobacteria and algae occurring in the Espan System do indeed show optimal growth in this range of concentrations or whether the iron content does not have a specific effect on growth needs to be investigated by future experiments that ideally would isolate the organisms from the water course in order to investigate them under varying Fe, pH and temperature conditions.

5 Author contribution

Inga Köhler, David Piatka and Johannes Barth carried out the sample collection and water analysis for on-site and isotope data. Raul Martinez carried out the calculation of the saturation index. Michelle Gehringer, Achim Herrmann and Arianna Gallo performed the analysis and interpretation of cyanobacteria and algae data. Inga Köhler prepared the manuscript with contributions from all co-authors

6 Acknowledgements

Funding for this project was made available by the German Research Foundation (DFG) in the Project IsoDO (BA 2207/15-1) awarded to Johannes Barth and GE2558/3-1 & GE2558/4-1 awarded to Michelle Gehringer. We also thank Christian Hanke, Marlene Dordoni and Marie Singer for help with sampling and analyses. The authors declare that they have no conflict of interest.

References

Andrews, S. C., Robinson, A. K., and Rodríguez- Quiñones, F.: Bacterial iron homeostasis, FEMS Microbiol. Rev., 27, 215-237, https://doi.org/10.1016/S0168-6445(03)00055-X, 2003.

Appelo, T., Van der Weiden, M. J., Tournassat, C., and Charlet, L.: Surface Complexation of Ferrous Iron and Carbonate on Ferrihydrite and the Mobilization of Arsenic, Environ. Sci. Technol., 36, 3096-3103, https://doi.org/10.1021/es010130n, 2002.

Armstrong, W., and Armstrong, J.: Stem photosynthesis not pressurised ventilation is responsible for light-enhanced oxygen supply to submerged roots of alder (Alnus glutinosa), Ann. Bot., 96, 591-612, https://doi.org/10.1093/aob/mci213, 2005.

Barth, J. A. C., Tait, A., and Bolshaw, M.: Automated analyses of O-18/O-16 ratios in dissolved oxygen from 12-mL water samples, Limnol. Oceanogr. Methods., 2, 35-41, https://doi.org/10.4319/lom.2004.2.35, 2004.

Bell, T. G., and Kramvis, A.: Fragment Merger: An Online Tool to Merge Overlapping Long Sequence Fragments, Viruses, 5, 824-833, https://doi.org/10.3390/v5030824, 2013.

Benson, B. B., and Krause D.: The concentration and isotopic fractionation of gases dissolved in freshwater in equilibrium with the atmosphere. 1. Oxygen, Limnol. Oceanogr., 25, 662-671, https://doi.org/10.4319/lo.1980.25.4.0662, 1980.

Büttner, G., Stichler, W., and Scholz M.: Hydrogeochemische Untersuchungen in den Forschungsbohrungen Lindau 1 und Spitzeichen 1 (Fränkisches Bruchschollenland), Geol. Bavar., 109, 105-124, 2006.

Brock T. D.: Lower pH limit for the existence of blue-green algae: evolutionary and ecological implications, Science, 179, 480-483, https://doi.org/0.1126/science.179.4072.480, 1973.

Caetano, M., and Vale, C.: Retention of arsenic and phosphorus in iron-rich concretions of Tagus salt marshes, Mar. Chem., 79, 261-271, https://doi.org/10.1016/S0304-4203(02)00068-3, 2002.

Clark, I. D. and Fritz, P. (Eds.): Environmental Isotopes in Hydrogeology, CRC Press/Lewis, Boca Raton, USA, 1997.

https://doi.org/10.5194/bg-2021-68
Preprint. Discussion started: 22 March 2021

Cornell, R. M. and Schwertmann, U. (Eds.): The Iron Oxides: Structure, Properties, Reactions, Occurrences and Uses, Wiley-VCH Verlag, Weinheim, Germany, 2003.

Eisenstadt, D., Barkan, E., Luz, B., and Kaplan, A.: Enrichment of oxygen heavy isotopes during photosynthesis in phytoplankton, Photosynth. Res., 103, 97-103, https://doi.org/10.1007/s11120-009-9518-z, 2010.

Gammons, C. H., Henne, W., Poulson, S. R., Parker, S. R ., Johnston, T. B., Dore, J. E., and Boyd, E. S.: Stable isotopes track biogeochemical processes under seasonal ice cover in a shallow, productive lake, Biogeochemistry, 120, 359–379, https://doi.org/10.1007/s10533-014-0005-z, 2014.

Gehringer, M. M., Pengelly, J. J. L., Cuddy, W. S., Fieker, C., Foster, P. I., and Neilan, B. A.: Host selection of symbiotic cyanobacteria in 21 species of the Australian cycad genus: Macrozamia (Zamiaceae), Mol. Plant. Microbe. Interact., 23, 811-822, https://doi.org/10.1094/MPMI-23-6-0811, 2010.

Guy, R. D., Fogel, M. L., and Berry J. A.: Photosynthetic fractionation of the stable isotopes of oxygen and carbon, Plant Physiol., 101, 37–47, https://doi.org/10.1104/pp.101.1.37, 1993.

Heidari, F., Zima, J., Riahi, H., and Hauer, T.: New simple trichal cyanobacterial taxa isolated from radioactive thermal springs, Fottea. Olomouc., 18, 137-149, https://doi.org/ 10.5507/fot.2017.024, 2018.

Jung, P., Briegel-Williams, L., Schermer, M., and Büdel, B.: Strong in combination: Polyphasic approach enhances arguments for cold-assigned cyanobacterial endemism, Microbiologyopen, 8, e00729, https://doi.org/10.1002/mbo3.729, 2019.

Kampbell, D. H., Wilson, J. T., and Vandegrift, S. A.: Dissolved-oxygen and methane in water by a Gc headspace equilibration technique, Int. J. Environ. Anal. Chem., 36, 249–257, https://doi.org/10.1080/03067318908026878, 1989.

Kappler, A., Bryce, C., Mansor, M., Lueder, U., Byrne, J. M., and Swanner, E. D.: An evolving view on biogeochemical cycling of iron, Nat. Rev. Microbiol., https://doi.org/10.1038/s41579-020-00502-7, 2021.

Knox, M., Quay, P. D., and Wilbur, D.: Kinetic isotopic fractionation during air-water gas transfer of O_2, N_2; CH_4, and H_2, J. Geophys. Res. Oceans, 97, 20335-20343, https://doi.org/10.1029/92JC00949, 1992.

Köhler, I., Piatka, D., Barth, J. A. C., and Martinez, R. E.: Beware of effect on isotopes of dissolved oxygen during storage of natural iron -rich water samples: A technical note, Rapid Commun. Mass Spectrom., 35, e9024, https://doi.org/10.1002/rcm.9024, 2020.

Komárek, J., and Anagnostidis, K.: Cyanoprokaryota. 2. Oscillatoriales, in: Süsswasserflora von Mitteleuropa, edited by: Büdel, B., Krienitz, L., Gärtner, G., and Schagerl, M., Elsevier/Spektrum, Heidelberg, Germany, 759, 2005.

https://doi.org/10.5194/bg-2021-68
Preprint. Discussion started: 22 March 2021

Kritzberg, E. S., and Ekström, S. M.: Increasing iron concentrations in surface waters- A factor behind brownification?, Biogeosciences Discuss., 8, 12285-12316, https://doi.org/10.5194/bg-9-1465-2012, 2011.

Kritzberg, E. S., Maher, Hasselquist, E., Skerlep, M., Löfgren, S., Olsson, O., Stadmark, J., Valinia, S., Hansson, L. A., and Laudon, H.: Browning of freshwaters: Consequences to ecosystem services, underlying drivers, and potential mitigation measures, Ambio., 49, 375-390, https://doi.org/10.1007/s13280-019-01227-5, 2020.

Kroppnick, P. M.: Respiration, photosynthesis, and oxygen isotope fractionation in oceanic surface waters, Limnol. Oceanogr., 20, 988-992, https://doi.org/10.4319/lo.1975.20.6.0988, 1975.

Liger, E., Charlet, L., and Van Cappellen, P.: Surface Catalysis of Uranium(VI) Reduction by Iron(II), Geochim. Cosmochim. Acta., 63, 2939-2955, https://doi.org/10.1016/S0016-7037(99)00265-3, 1999.

Llyod, R. M.: Oxygen isotope behavior in the Sulfate-Water System, J. Geophys. Res., 73, 6099-6110, https://doi.org/10.1029/JB073i018p06099, 1968.

Lu, J. -B. Jian, J., Huang, W., Lin, H., Li, J., and Zhou, M.: Experimental and theoretical identification of the Fe(VII) oxidation state in FeO_4^-, Phys. Chem. Chem. Phys., 18, 31125-31131, https://doi.org/10.1039/C6CP06753K, 2016.

Mader, M., Schmidt, C., van Geldern, R., and Barth, J. A. C.: Dissolved oxygen in water and its stable isotope effects: A review, Chem. Geol., 473, 10-21, https://doi.org/10.1016/j.chemgeo.2017.10.003, 2017.

Mader, M., Roberts, A. M., Porst, D., Schmidt, C., Trauth, N., van Geldern, R., and Barth, J. A. C.: River recharge versus O_2 supply from the unsaturated zone in shallow riparian groundwater: A case study from the Selke River (Germany), Sci Total Environ., 634, 374-381, https://doi.org/10.1016/j.scitotenv.2018.03.230, 2018.

Michaud, S. C., and Richardson, C. J.: Relative radial oxygen loss in five wetland plants, in: Constructed Wetlands for Wastewater Treatment, edited by: Hammer, D. A., Lewis Publishers, Chelsea, USA, 501–507, 1989.

Millero, F. J.: The effect of ionic interactions on the oxidation of metals in natural waters, Geochim. Cosmochim. Acta., 49, 547–53, https://doi.org/10.1016/0016-7037(85)90046-8, 1985.

Oba, Y., and Poulson, S. R.: Oxygen isotope fractionation of dissolved oxygen during reduction by ferrous iron, Geochim Cosmochim Acta., 73, 13-24, https://doi.org/10.1016/j.gca.2008.10.012, 2009.

Oba, Y, and Poulson, S. R.: Oxygen isotope fractionation of dissolved oxygen during abiological reduction by aqueous sulfide, Chem Geol., 268, 226-232, https://doi.org/10.1016/j.chemgeo.2009.09.002, 2009.

Park, B., and Dempsey, B. A.: Heterogeneous oxidation of Fe(II) on ferric oxide at neutral pH and a low partial pressure of O_2, Environ. Sci. Technol., 39, 6494–6500, https://doi.org/10.1021/es0501058, 2005.

https://doi.org/10.5194/bg-2021-68
Preprint. Discussion started: 22 March 2021

Parker, S. R., Poulson, S. R., Gammons, C. H., and DeGrandpre, M. D.: Biogeochemical controls on diel cycling of stable isotopes of dissolved oxygen and dissolved inorganic carbon in the Big Hole River, Montana, Environ Sci Technol., 39, 7134–7140, https://doi.org/10.1021/es0505595, 2005.

Parker, S. R., Gammons, C. H., Poulson, S. R., DeGrandpre, M. D., Weyer, C. L., Smith, M. G., Babcock, J. N., and Oba, Y.: Diel behavior of stable isotopes of dissolved oxygen and dissolved inorganic carbon in rivers over a range of trophic conditions, and in a mesocosm experiment, Chem Geol., 269, 22–32, https://doi.org/10.1016/j.chemgeo.2009.06.016, 2010.

Parker, S. R., Gammons, C. H., Smith, M. G., and Poulson, S. R.: Behavior of stable isotopes of dissolved oxygen, dissolved inorganic carbon and nitrate in groundwater at a former wood treatment facility containing hydrocarbon contamination, Appl. Geochem., 27, 1101-1110, https://doi.org/10.1016/j.apgeochem.2012.02.035, 2012.

Parker, S. R., Darvis, M. N., Poulson, S. R., Gammons, C. H., and Stanford, J. A.: Dissolved oxygen and dissolved inorganic carbon stable isotope composition and concentration fluxes across several shallow floodplain aquifers and in a diffusion experiment, Biogeochemistry, 117, 539-552, https://doi.org/10.1007/s10533-013-9899-0, 2014.

Parkhurst, D. L., and Appelo, C. A. J.: Description of input and examples for PHREEQC version 3–A computer program for speciation, batch-reaction, one-dimensional transport, and inverse geochemical calculations. Volume book 6 series Techniques and Methods. 2009.

Pati, S. G., Bolotin, J., Brennwald, M. S., Kohler, H. P. E., Werner, R. A., and Hofstetter, T. B.: Measurement of oxygen isotope ratios ($^{18}O/^{16}O$) of aqueous O_2 in small samples by gas chromatography/isotope ratio mass spectrometry, Rapid Commun. Mass Spectrom., 30, 684–690, https://doi.org/10.1002/rcm.7481, 2016.

Pusch, M.: The metabolism of organic matter in the hyporheic zone of a mountain stream, and its spatial distribution, Hydrobiologia, 323, 107-118, https://doi.org/10.1007/BF00017588, 1996.

Quay, P. D., Wilbur, D. O., Richey, J. E., Devol, A. H., Benner, R., and Forsberg, B. R.: The ^{18}O:^{16}O of dissolved oxygen in rivers and lakes in the Amazon Basin: Determining the ratio of respiration to photosynthesis rates in freshwater. Limnol. Oceanogr., 40, 718-729, https://doi.org/10.4319/lo.1995.40.4.0718, 1995.

Schwertmann, U.: Solubility and dissolution of iron oxides, Plant Soil, 130, 1-25, https://doi.org/10.1007/BF00011851, 1991.

Schwab, R. G.: Die natürliche Radioaktivität der Erdkruste, in: Natürliche und künstliche Strahlung in der Umwelt. Eine Bilanz vor und nach Tschernobyl, edited by: Hosemann, G., and Wirth, E., Erlanger Forschungen Reihe B, Erlangen, Germany, 25-43, 1987.

https://doi.org/10.5194/bg-2021-68
Preprint. Discussion started: 22 March 2021

Sylvester, P., Westerhoff, P., Boyd, O., and Sengupta, A. K.: Arsen X^{np} - A new hybrid sorbent for arsenic removal from drinking water, in: ACE '05, Proceedings of the AWWA Annual Conference and Exposition, San Francisco; USA, 2005.

Skinner, B.J.: A Second Iron Age Ahead? Res. J. Environ. Sci., 3, 559-575, https://doi.org/10.1016/S0166-1116(08)71071-9, 1979.

Smith, L., Watzin, M. C., and Druschel, G.: Relating sediment phosphorus mobility to seasonal and diel redox fluctuations at the sediment-water interface in a eutrophic freshwater lake. Limnol. Oceanogr., 56, 2251-2264, https://doi.org/10.4319/lo.2011.56.6.2251, 2011.

Stanier, R. Y., Kunisawa R., Mandel, M., and Cohen-Bazire, G.: Purification and properties of unicellular blue-green algae (order Chroococcales). Bacteriol. Rev. 35, 171-205, https://doi.org/10.1128/mmbr.35.2.171-205.1971, 1971.

Swanner, E. D., Mloszewska, A. M., Cirpka, O. A., Schoenberg, R., Konhauser, K. O., and Kappler, A.: Modulation of oxygen production in Archaean oceans by episodes of Fe(II) toxicity, Nat. Geosci., 8, https://doi.org/10.1038/ngeo2327, 126–130, 2015.

Taylor, B. E., and Wheeler, M. C.: Sulfur- and Oxygen-Isotope Geochemistry of Acid Mine Drainage in the Western United States, in: Environmental Geochemistry of Sulfide Oxidation edited by: Alpers, C. N., and Blowes, D. W., American Chemical Society Symposium Series, Washington DC, USA, 481-514, 1993.

Teal, J. M. and Kanwisher, J. W.: Gas Transport in the Marsh Grass, Spartina alterniflora, J. Exp. Bot., 17, 355-361, https://doi.org/10.1093/jxb/17.2.355, 1966.

van Geldern, R. and Barth, J. A. C.: Optimization of instrument setup and post-run corrections for oxygen and hydrogen stable isotope measurements of water by isotope ratio infrared spectroscopy (IRIS), Limnol. Oceanogr. Methods, 10, 1024-1036, https://doi.org/10.4319/lom.2012.10.1024, 2012.

Wand, X., and Veizer, J.: Respiration-photosynthesis balance of terrestrial aquatic ecosystems, Ottawa area, Canada. Geochim. Cosmochim. Acta., 64, 3775-3786, https://doi.org/10.1016/S0016-7037(00)00477-4, 2000.

Wassenaar, L. I., and Koehler, G.: An on-line technique for the determination of the $\delta^{18}O$ and $\delta^{17}O$ of gaseous and dissolved oxygen, Anal. Chem., 71, 4965–4968, https://doi.org/10.1021/ac9903961, 1999.

Wassenaar, L. I.,and Hendry, M. J.: Dynamics and stable isotope composition of gaseous and dissolved oxygen, Ground Water, 45, 447–460, https://doi.org/10.1111/j.1745-6584.2007.00328.x, 2007.

https://doi.org/10.5194/bg-2021-68
Preprint. Discussion started: 22 March 2021

Weyhenmeyer, G. A., Prairie, Y. T., and Tranvik, L. J.: Browning of Boreal Freshwaters Coupled to Carbon-Iron Interactions along the Aquatic Continuum, PLoS One, 9, e88104, https://doi.org/10.1371/journal.pone.0088104, 2014.

Wilmotte, A., Van der Auwera, G., and De Wachter, R.: Structure of the 16S ribosomal RNA of the thermophilic cyanobacterium Chlorogloeopsis HTF (Mastigocladus laminosus HTF') strain PCC75 18, and phylogenetic analysis, FEBS Lett., 317, 96–100, https://doi.org/10.1016/0014-5793(93)81499-p, 1993.

Zhang, Y., Charlet, L., and Schindler P. W.: Adsorption of protons, Fe(II) and Al(III) on lepidocrocite (γ-FeOOH), Colloids Surf., 63, 259-268, https://doi.org/10.1016/0166-6622(92)80247-Y, 1992.